Odor-evoked calcium signals in dendrites of rat mitral cells

Serge Charpak*†, Jerome Mertz*, Emmanuel Beaurepaire*, Laurent Moreaux*, and Kerry Delaney*†‡

*Laboratoire de Neurophysiologie, Institut National de la Santé et de la Recherche Médicale, EPI0002, Ecole Supérieure de Physique et Chimie Industrielles de la Ville de Paris, 10 Rue Vauquelin, 75231 Paris, France; and ‡Department of Biological Sciences, Simon Fraser University, Burnaby, BC, Canada V5A 1S6

Edited by Per O. Andersen, University of Oslo, Oslo, Norway, and approved November 22, 2000 (received for review September 5, 2000)

Mitral cell dendrites do more than passively integrate and convey synaptic potentials to the soma, they release transmitter onto local interneurones to mediate recurrent and lateral inhibition. Several mechanisms may control the level of dendritic intracellular calcium ($[Ca^{2+}]$) and define timing for dendritic release. Here we investigated *in vivo*, how odor controls calcium dynamics in mitral cell dendrites by combining intracellular recording and two-photon microscopy imaging of $[Ca^{2+}]$. During odor stimulation, two types of $[Ca^{2+}]$ changes accompany membrane potential oscillations that are phase-locked with the respiratory cycle: (*i*) one is graded and parallels the membrane potential, even below the threshold for action potential firing; (*ii*) a second is transient, triggered by sodium action potentials that invade the entire dendritic tree. These results indicate that mitral cell dendritic compartments are synchronized by action potentials and suggest that the efficacy of dendritic synapses is finely tuned by odor-evoked graded changes in $[Ca^{2+}]$.

In many neurons, voltage-dependent regenerative sodium and calcium currents participate in transferring excitatory synaptic inputs from distal dendrites to the soma or, inversely, in propagating sodium action potentials backward to varying extents into dendrites (1). *In vitro*, these back-propagating action potentials have been proposed to be involved in numerous synaptic processes (2–5), including transmitter release (6). In mitral cells, dendritic action potentials (7–10) could define a precise timing for dendritic release upon local interneurones. Moreover, because the sites of synaptic inputs are located near dendritic release sites, the possibility of graded release (11, 12) or synaptic modulation of action potential-evoked release should also be considered. *In vivo* measurements of neuronal function are however needed to complement slice studies because the "environment" in which a neuron operates is different from that in an *in vitro* slice; e.g., the temperature is higher, cells are constantly bombarded with synaptic potentials, etc., and these factors have been shown in some cases to strongly influence whether synaptic depolarization and sodium action potentials (13, 14) trigger dendritic $[Ca^{2+}]$ changes. As well, natural stimulation of the sensory receptors generates a specific temporal and spatial pattern of synaptic inputs to neurons that cannot be reproduced in slices (15, 16). Some of the data have been presented in preliminary form.[§]

Methods

***In Vivo* Electrophysiology and Odor Stimulations.** Wistar rats, P30-P45, were anesthetized with 1.5 mg/kg urethane i.p. and held in a standard stereotaxic apparatus with ear bars. Atropine 0.5 mg/kg i.p. was injected at the onset of anesthesia and supplemented at approximately hourly intervals at 0.1 mg/kg. Xylocaine paste (2%) was applied to the ear bars and skin before surgery and to the cut edges of the skin after exposure of the cranial bone. In some experiments, the posterior cisterna was drained. A craniotomy was performed above one bulb hemisphere, and the dura was removed. Before the removal of the bone and dura, a fiberglass frame was attached to the skull with dental cement with an opening over the bone above the olfactory bulb. After removal of the dura, a recording micropipette was positioned at the surface of the bulb, a 100-μm-thick glass coverslip was placed on the fiberglass frame, and the space below the glass was filled with a 3% agar solution. The temperature of the animal was monitored with a rectal thermometer and maintained at 36°C–37°C by using a feedback controlled heating blanket (Harvard Apparatus, Holliston, MA). Borosilicate glass micropipettes, 1.5 mm o.d. × 0.86 mm i.d. were filled with a solution of 3 mM Ca^{2+}-Green-1 in 2 M or 1 M potassium acetate (pipette resistances with 1 M potassium acetate were 80–120 Mohm). The dye was injected with continuous hyperpolarizing current of approximately 0.5 nA for 10 to 30 min. Electrophysiological signals recorded with an intracellular microelectrode amplifier (Neurodata, Cygnus Technology, Delaware Water Gap, PA) were digitized and stored on a personal computer (Digidata 1200A; Clampex 8, Axon Instruments, Foster City, CA). In addition, electrophysiological data were simultaneously acquired and synchronized to the images with custom LABVIEW-based software at a sampling rate of 5–10 kHz with 8-bit resolution. A continuous stream of humidified air was applied from a storage cylinder and directed over the nose with a Teflon cone. Odor was applied for durations of 0.5 to 6 seconds (typically 3 or 4 seconds) by switching the air delivery to a 60-ml reservoir containing filter paper soaked in pure amyl acetate with a solenoid-controlled valve (Lee Valve, Westbrook, CT). Teflon tubing was used (from the odor reservoir to the nose).

***In Vivo* Two-Photon Imaging.** Ca^{2+}-Green-1 fluorescence was excited and imaged by using a custom built two-photon laser scanning microscope. Prechirped 830-nm excitation from a femtosecond-pulsed laser (Spectra-Physics Tsunami; 5-W pump) was focused onto filled neurons by using a ×63 Leica water immersion objective. Up to 290 mW of power into the sample was needed to image somata and basal dendrites up to 450 μm below the pial surface. The back aperture was 20% under-filled to increase excitation power and slightly decrease spatial resolution in the *z*-direction. Galvanometric scanning (GS120, General Scanning, Watertown, MA) controlled by home built electronics and software (LABVIEW) was used to obtain repetitive single line scans at rates between 300 and 1000 lines per second or images from subregions of the field of view at rates up to 100 fps. A background fluorescence value was obtained by averaging pixels from an unstained region of the tissue. Rectangular zones of interest in the image containing dye-filled structures were chosen for analysis. Normalized fluorescence changes were

This paper was submitted directly (Track II) to the PNAS office.

†To whom reprint requests should be addressed. E-mail: serge.charpak@espci.fr or kdelaney@sfu.ca.

§Charpak, S., Mertz, J., Moreaux, L., Beaurepaire, E. & Delaney, K. R. (1999) *Soc. Neurosci. Abstr.,* abstr. 55.2.

The publication costs of this article were defrayed in part by page charge payment. This article must therefore be hereby marked "*advertisement*" in accordance with 18 U.S.C. §1734 solely to indicate this fact.

Article published online before print: *Proc. Natl. Acad. Sci. USA*, 10.1073/pnas.021422798. Article and publication date are at www.pnas.org/cgi/doi/10.1073/pnas.021422798

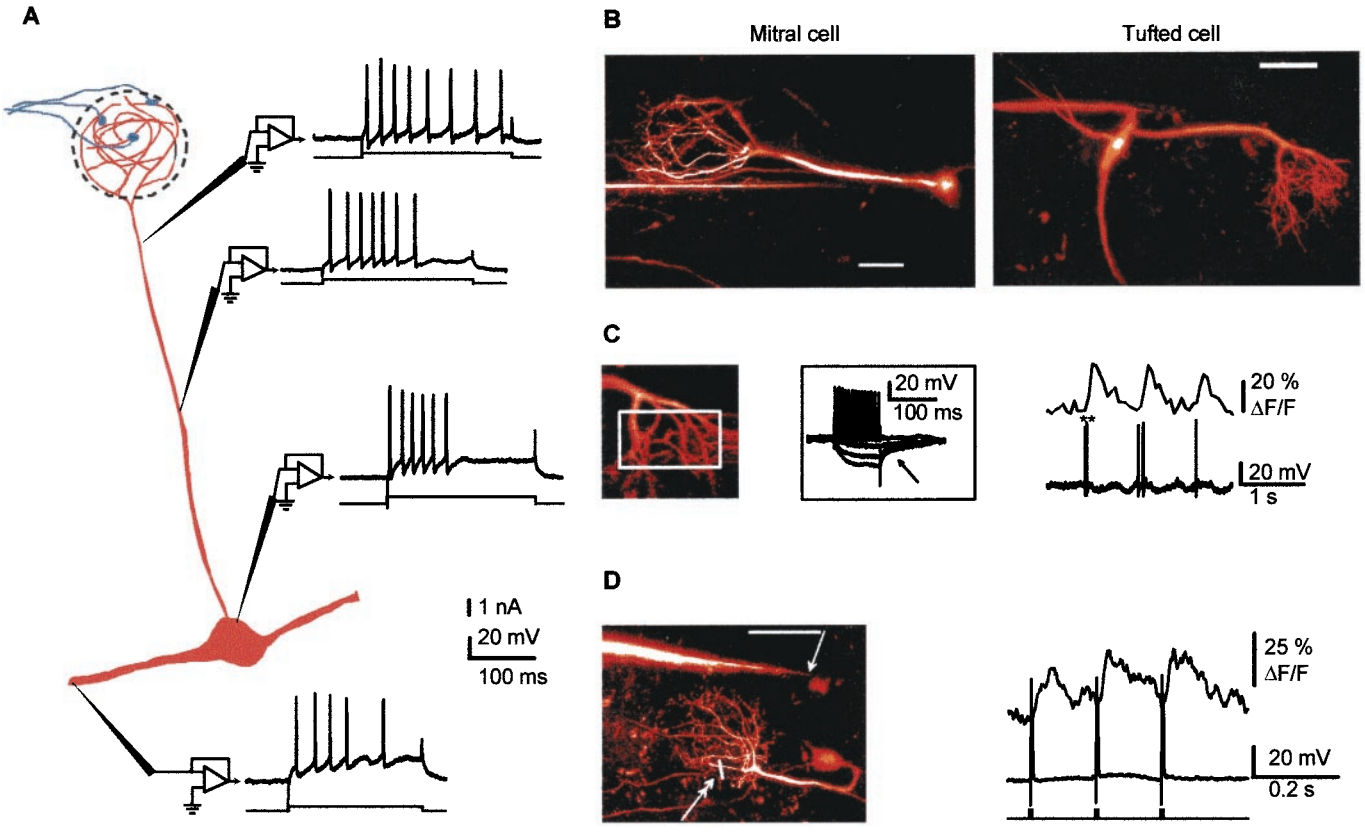

Fig. 1. Sodium action potentials synchronize [Ca^{2+}] transients in all dendritic compartments of mitral cells in the olfactory bulb of anesthetized rats. (*A*) Fast sodium action potentials were observed with sharp electrode recordings from apical secondary dendrites and from the soma. Shown is a schematic diagram of mitral cell synaptic connections and responses from four different mitral cells to depolarizing current pulses. Sodium action potentials were seen at all sites. Note that the resting membrane potential and the injected currents varied slightly at each site. (*B*) Examples of mitral and tufted cells that were filled with Ca^{2+}-Green-1 and imaged using two-photon microscopy (see *Methods* for recording and imaging techniques). Both pictures are two-dimensional projections of image stacks (up to 200 frames each separated by a 2-μm step in depth) obtained at the end of the recording session (scale bars = 50 μm). Electrophysiological recordings were obtained from the soma (*Left*, mitral cell, length of the apical dendrite, 210 μm) and at the origin of a secondary dendrite (*Right*, tufted cell, length of the apical dendrite, 130 μm). (*C*) Spontaneous action potentials induce a [Ca^{2+}] rise in the tuft. (*Left*) Fluorescence signals indicative of [Ca^{2+}] changes were integrated in the region indicated by a white rectangle (same tufted cell as in *B*; the ** indicates a spike doublet). The *Inset* Illustrates the firing of the cell for which hyperpolarizing pulses activated an I_A-type current (arrow). (*D*) Action potentials propagate backward *in vivo*. (*Left*) A recording micropipette was placed in the secondary dendrite (arrow) of a mitral cell with a long apical dendrite (230 μm, scale bar = 50 μm), and fluorescence signals were measured in two tuft branchlets (double arrow) by using a line scan. (*Right*) Three single spikes, evoked with depolarizing current pulses (1.5 nA, 5 ms) injected in the secondary dendrite, induce fast [Ca^{2+}] transients in the tuft. Because of the location of the current injection site distal to the soma, it is most likely that sodium action potentials were initiated in the secondary dendrite or possibly in the soma and propagated backward to the tuft (i.e., they did not initiate in the tuft dendrite). Note the rapid decay of the transient elicited by a single action potential.

calculated as $\Delta F/F = (F_n - F_0)/(F_0)$, where F_n is the background corrected average intensity within the measurement box in frame n and F_0 is the background corrected average intensity averaged over five frames at the start of a sequence. Where it was necessary to correct for dye fading during the recording, an exponential function was fitted to the fluorescence data from the initial 1–2 s of the sequence, and the raw fluorescence data were corrected for fading before the calculation of $\Delta F/F$.

Results

We have combined two-photon laser scanning microscopy (TPLSM) (18) of Ca^{2+}-Green-1 fluorescence and intracellular recordings to investigate the properties of mitral cell dendrites in anesthetized rats during odor stimulation. We focused the study on Ca^{2+} signals in the distal apical dendrite tuft, which behaves both as a postsynaptic structure that receives olfactory receptor cell terminals and as a presynaptic structure that releases transmitter onto local interneurones (19). Ca^{2+} changes in the tuft could therefore reflect the cell firing (14, 20–22) and the activation of postsynaptic receptors, as well as the properties of a dendritic release site. Intracellular recordings ($n = 35$) with stable membrane potentials of −55 mV or greater were obtained from mitral and tufted cells (Fig. 1*B*). The location of the recording was obtained by TPLSM imaging of the micropipette tip to reveal that about 70% ($n = 24$) of the cells were impaled in a dendrite rather than in the soma. Fast sodium action potentials were systematically observed regardless of the recording site. The firing behavior with regard to action potential shape, amplitude, firing rate, and after-potentials was very similar in recordings from somata and all locations along the apical ($n = 18$) and secondary dendrites ($n = 6$) (up to 300 μm distal to the soma, Fig. 1*A*). Slow rising, or sustained Ca^{2+} action potentials were not seen in response to brief or prolonged depolarizing current injections. Repetitive firing induced by a few hundred ms of current injection showed little evidence for attenuation of spike amplitude. *In vivo*,mitral cell dendrites thus possess regenerative membrane properties similar to those of an axon, with little evidence for regulation of the conductive properties of the apical dendrite by K^+ currents or Na^+ channel inactivation (23, 24).

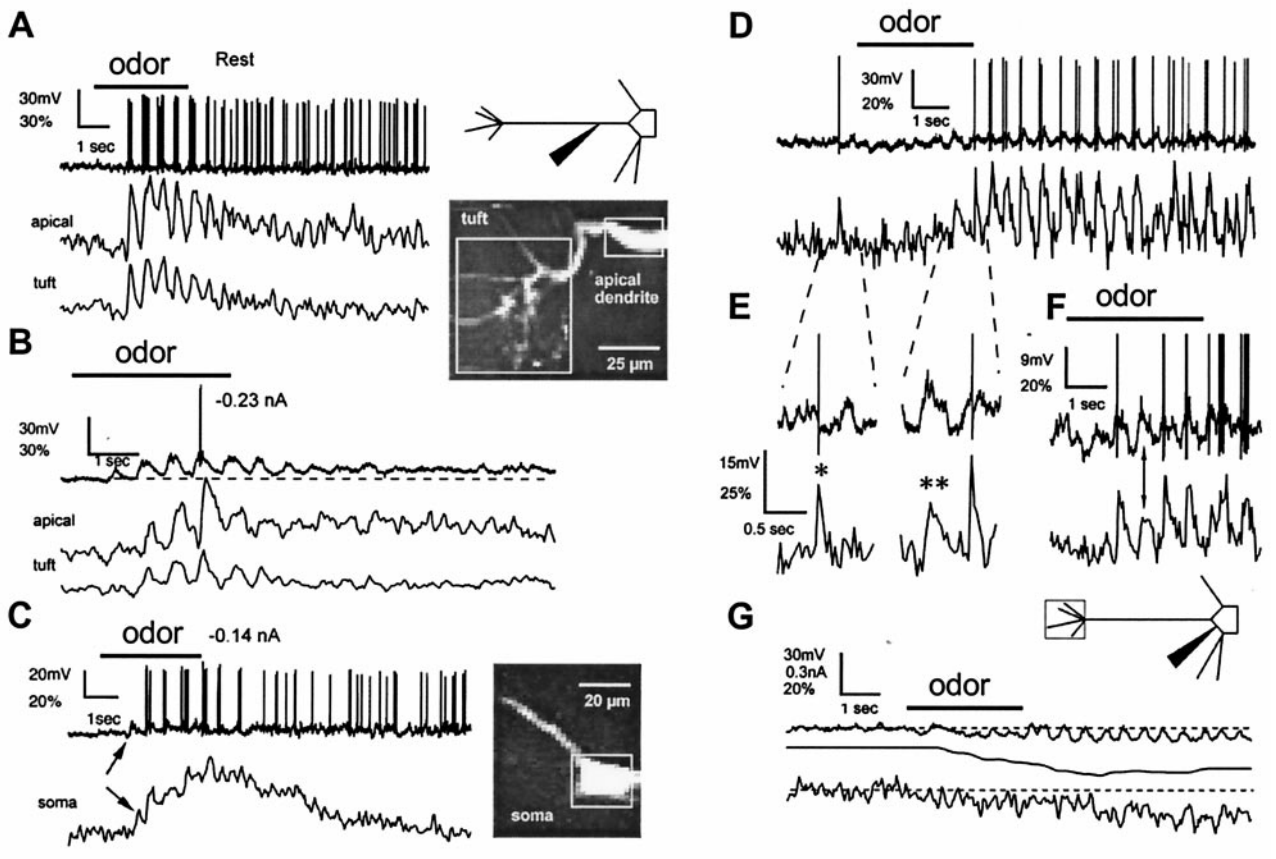

Fig. 2. Odor stimulation evokes two types of $[Ca^{2+}]$ changes in mitral cell dendrites. (*A–C*) Fluorescence measurements from the distal tuft, the apical dendrite at the edge of the glomerulus (200 μm from the soma), and the soma of a cell. The microelectrode was located in the apical dendrite 75 μm distal to the soma. (*A Left*) During odor stimulation (3 s isoamyl acetate), transient $[Ca^{2+}]$ increases were observed, phase-locked with bursts of action potentials that occurred during each respiratory cycle. $[Ca^{2+}]$ increases recovered substantially between breaths. (*B*) Subthreshold depolarizations evoke $[Ca^{2+}]$ changes. Hyperpolarization of membrane potential below the threshold for spike generation revealed underlying cyclical depolarizations during odor presentation. In both the apical tuft and dendrite, subthreshold slow depolarizations were co-incident with increases in $[Ca^{2+}]$. Dashed line below voltage trace highlights the sustained depolarization after odor offset. (*C*) Increased $[Ca^{2+}]$ during odor-evoked subthreshold depolarization was also seen in the soma (same cell, apical dendrite projecting toward left and top). Vertical arrow indicates an increase in $[Ca^{2+}]$, which begins with the first subthreshold depolarization (fluorescence changes expressed as $\Delta F/F$%). (*D–G*) Voltage dependency of depolarization- and action potential-evoked $[Ca^{2+}]$ increases in fine tuft dendrites. The microelectrode was located in the soma of another cell. (*D*) The mixed response to application of the odor was initially inhibitory overall but became excitatory toward the end of application with one subthreshold depolarization inducing a slow $[Ca^{2+}]$ increase (see below). (*E*) Expanded portion of records in *D* as indicated shows the rapid recovery kinetics of $\Delta[Ca^{2+}]$ provoked by action potentials (*) compared with subthreshold voltage depolarizations (**). (*F*) Another odor application in the same cell. (*G*) A large hyperpolarization blocks all $[Ca^{2+}]$ changes. Hyperpolarizing current (middle trace) was progressively injected to oppose the increasing odor-induced excitation. $[Ca^{2+}]$ increases in phase with respiration-linked slow depolarizations were no longer observed. Instead, a reduction in the steady-state $[Ca^{2+}]$ level occurred.

We next investigated whether sodium action potentials evoked $[Ca^{2+}]$ increases in mitral cell dendrites. Spontaneous and current-evoked action potentials induced rapid onset $[Ca^{2+}]$ transients throughout the cell (the distal tuft, the apical and the secondary dendrites, and the soma). Fig. 1*C* shows fast $[Ca^{2+}]$ transients in a distal apical tuft that were correlated with spontaneous action potentials recorded at the origin of the secondary dendrite of a tufted cell. The initiation site of a spontaneous action potential cannot be determined in the absence of simultaneous dual-site recording from different parts of the same cell (1, 9). Taking advantage of the combination of TPLSM and intracellular recording, we could, however, demonstrate action potential propagation in dendrites. We recorded the fluorescence transients evoked in the apical dendrite or in fine branches of the apical tuft ($n = 4$) in response to a depolarizing current injection located in secondary dendrites. With this protocol, action potentials were most likely initiated in the secondary dendrite or in the soma but not in the apical tuft (25). Fig. 1*D* illustrates that an action potential initiated in deep layers could propagate backward to the glomerular tuft and induce a $[Ca^{2+}]$ transient that peaked within 10 msec of onset and recovered smoothly to baseline within 100 to 200 ms. Because action potentials evoked with a current injection in the apical dendrite also caused $[Ca^{2+}]$ transients in secondary dendrites (up to 300 μm from the soma, not shown), we conclude that mitral cell dendritic compartments are synchronized during a single action potential.

We then investigated the origin and kinetics of the $[Ca^{2+}]$ variations that occur during an odor-induced excitation. Inhalation of isoamyl acetate induced various types of excitatory, mixed excitatory/inhibitory, or inhibitory responses (nonresponsive cells were discarded before dye filling). Excitatory odor responses were characterized by synaptic depolarization phase-locked to the respiratory cycle and upon which were superimposed bursts of action potentials (Fig. 2*A*). As expected, each burst of action potentials was accompanied by a phasic $[Ca^{2+}]$ increase in all cell compartments. In the somata, the kinetics of Ca^{2+} removal was slow compared with the breathing rate so that Ca^{2+} accumulated throughout the period of odor exposure (Fig. 2C). However, in the small tuft dendrites, the recovery kinetics

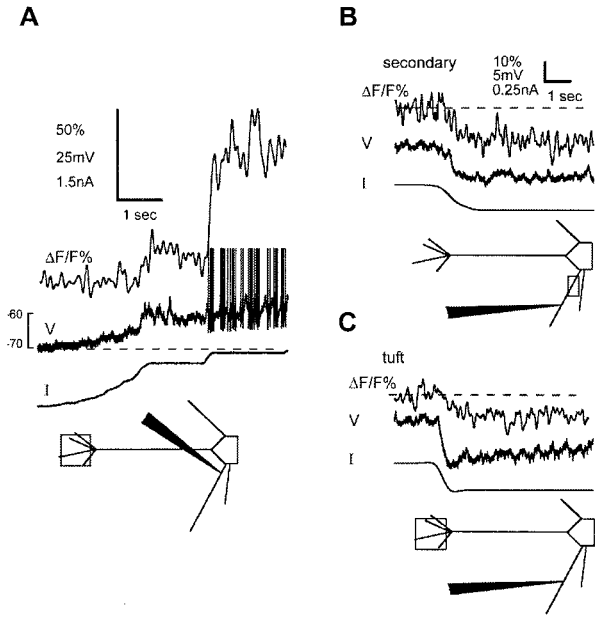

Fig. 3. The steady $[Ca^{2+}]$ level is modulated by membrane potential below rest. Top traces in each panel are $\Delta F/F\%$, middle are membrane potential, and bottom are dc current. (*A*) Depolarization of the mitral cell from approximately −73mV to below the action potential threshold is accompanied by an increase in the steady $[Ca^{2+}]$. The current injection site was located in a secondary dendrite, and $[Ca^{2+}]$ was measured in the tuft. The action potentials are truncated (*B* and *C*); hyperpolarization from threshold by 5–8 mV reduced the steady $[Ca^{2+}]$ level in both the secondary dendrite (*B*) (near the recording electrode) and the tuft (*C*) of another cell. Dashed line indicates resting fluorescence levels before changing the membrane potential, and scale bar in *B* applies to *C*.

were fast enough that changes in $[Ca^{2+}]$ faithfully followed the increase and decrease of electrical activity during each respiratory cycle, with only a little summation over the course of several breaths (Fig. 2 *A* and *B*).

Sensory afferents excite mitral cell tufts through glutamate receptor activation and subsequent membrane depolarization, which could possibly cause $[Ca^{2+}]$ changes independent of the occurrence of action potentials. To check for subthreshold Ca^{2+} increases, we reapplied the odor while the cell membrane potential was maintained hyperpolarized just below the firing threshold by injection of current through the recording electrode. Blocking action potentials this way revealed substantial $[Ca^{2+}]$ increases in the tuft branches, the apical dendrite, and the soma that followed the odor-induced, respiration-locked, subthreshold synaptic depolarizations (Fig. 2*B*). In some instances, the onset of subthreshold Ca^{2+} influx appeared to coincide with the occurrence of membrane potential oscillations in the gamma range (see Fig. 2*B*) that appeared similar to those described *in vitro* by Desmaisons *et al.* (26).

The voltage dependence of the subthreshold $[Ca^{2+}]$ changes was investigated in other cells (e.g., Fig. 2 *D–G* and Fig. 3). In Fig. 2 *D–G*, both action potentials and subthreshold synaptic depolarizations contributed to the $[Ca^{2+}]$ increases, although with different kinetics (Fig. 2*E*, see single and double asterisks). When the odor was applied while the cell membrane potential was set negative to −60 mV, the respiration-locked synaptic depolarizations remained but the subthreshold $[Ca^{2+}]$ fluctuations disappeared (Fig. 2*G*) and the steady-state level of $[Ca^{2+}]$ decreased (see also Fig. 3). We conclude that subthreshold $[Ca^{2+}]$ changes result from the opening of voltage-dependent Ca^{2+} channels in response to the membrane depolarization caused by non-*N*-methyl-D-aspartate (NMDA) glutamate receptor activation. The involvement of metabotropic (27) or NMDA glutamate receptors (28, 29) is unlikely because the $[Ca^{2+}]$ changes also occurred in the soma (Fig. 2*C*, arrow) and in the basal portion of the apical dendritic shaft, which are devoid of glutamatergic inputs (30).

Odor-evoked subthreshold depolarizations lasted for hundreds of milliseconds and were paralleled by dendritic $[Ca^{2+}]$ changes. The fact that brief $[Ca^{2+}]$ transients that followed single action potentials recovered within 100 ms or less in the finest tuft branches indicates that the time courses of subthreshold $[Ca^{2+}]$ increases are determined by a sustained Ca^{2+} influx into the cytoplasm and not by slow removal kinetics. Manipulation of the membrane potential with dc hyperpolarizing and depolarizing current injections, in the absence of sensory stimulation, revealed that cytoplasmic resting $[Ca^{2+}]$ was modulated within a range of 5–10 mV below threshold (Fig. 2*G*; Fig. 3). Fig. 3*A* shows that a sustained and moderate depolarization of a secondary dendrite below threshold could depolarize the tuft branchlets and cause a similarly sustained rise in $[Ca^{2+}]$. The changes in cytoplasmic $[Ca^{2+}]$ could be maintained for seconds or minutes, indicating that the currents involved were persistent.

Discussion

What are the possible functional implications of our observations? Our *in vivo* study establishes that initiation or propagation of dendritic sodium-dependent action potentials appears to be the default condition for mitral cell dendrites. These cells thus clearly differ from neocortical pyramidal cells that have been studied *in vivo*. In layer II/III pyramids, sodium action potentials rapidly decrease in amplitude with distance from the soma whereas, in deep pyramids, sodium action potentials propagate to the main bifurcation where they are relayed by complex spikes that invade the tuft (14, 22, 31). As opposed to these cells and others such as olivary or purkinje cells, the density of sodium channel must be quite homogenous in mitral cell dendrites (32, 33). Whether an action potential initiates distal or proximal to the soma of mitral cells is probably of lesser importance than the fact that propagation throughout the dendrites is reliable, at least for single action potentials under conditions of minimal synaptic inhibition. This global propagation will serve to electrically synchronize the anatomically separated dendritic compartments of the cell. This does not, however, preclude independent local modulation of action potential propagation in either the basal or distal apical dendrites, e.g., by local inhibition (34). $[Ca^{2+}]$ transients evoked by single action potentials decay rapidly in small tuft dendrites so repetitive firing at rates in excess of 10 Hz are required to obtain significant summation of action potential $[Ca^{2+}]$ transients to raise average cytoplasmic $[Ca^{2+}]$. These high firing rates are not typically observed in the absence of odor stimulation in non-anesthetized (35) or in urethane-anesthetized rats. However, some summation of action potential-associated $[Ca^{2+}]$ transients will occur during respiratory cycles when odor-evoked gamma oscillations drive firing to high frequencies.

With odor stimulation, we observed graded $[Ca^{2+}]$ increases that were synchronized to the respiration cycles and could be observed even in the absence of action potential firing. These increases could theoretically result from flux through ligand- or voltage-gated channels or release from internal stores. However, the voltage dependency of the $[Ca^{2+}]$ increases, as well as their presence in the apical dendrite and soma, regions devoid of synaptic inputs (30), suggest that they result from a low threshold voltage-activated Ca^{2+} window current operating within a potential range where inactivation and activation curves are overlapping (12, 36). Although the amplitudes of the subthreshold depolarizations were small compared with the action potentials, they were very effective in increasing average cytoplasmic $[Ca^{2+}]$ because they are sustained for hundreds of milliseconds throughout the respiratory cycle.

The low threshold activated Ca^{2+} window current, and the rapid Ca^{2+} removal kinetics produce a situation where cytoplasmic $[Ca^{2+}]$ is effectively a continuous function of membrane potential near rest. "Residual" $[Ca^{2+}]$ at mitral cell dendritic release sites is likely to increase synaptic efficacy, as seen in numerous other synapses (37–40). Depending on the physical coupling between the Ca^{2+} influx and releasable vesicles, this graded Ca^{2+} increase could either drive transmitter release directly (11, 12) or play a role in modulating action potential-evoked release. The increase of synaptic efficacy at dendrodendritic synapses will favor the synchronization of both periglomerular and granular networks by an action potential initiated locally or propagating backward. Whether it affects the temporal response pattern to odor of single mitral cells remains to be established (17).

In our experiments, respiration rates of about two per second, which are also typical for resting awake rats, produced little summation of $[Ca^{2+}]$ between breaths. However, when a rat is actively searching for an odor source, it produces periods of rapid, repeated inspirations, "sniffs" at a frequency of 5–7 Hz (35). The summation of the subthreshold Ca^{2+} increases would be predicted to be particularly dramatic during sniffing when inspiration frequency rises to a rate that equals or exceeds the intrinsic removal rate of Ca^{2+} from the dendrites and may play an important role in increasing sensitivity for odor detection or discrimination.

We thank B. Strowbridge, D. Kleinfeld, E. Audinat, and R. Malenka for comments on the manuscript. Support was provided by the Medical Research Council (Canada) and the French Embassy (to K.D.), the Institut National de la Santé et de la Recherche Médicale (INSERM), the Ministère de l'Education Nationale de la Recherche et de la Technologie (MENRT), and the Institut Curie. Part of the work was done when E.B. was supported by the Centre National de la Recherche Scientifique (UMR7637, CNRS). L.M. is on Centre National de la Recherche Scientifique-BDI Fellowship UPR5.

1. Stuart, G. J. & Sakmann, B. (1994) *Nature (London)* **367,** 69–72.
2. Markram, H., Helm, P. J. & Sakmann, B. (1995) *J. Physiol. (London)* **485,** 1–20.
3. Markram, H., Lubke, J., Frotscher, M. & Sakmann, B. (1997) *Science* **275,** 213–215.
4. Magee, J. C. & Johnston, D. (1997) *Science* **275,** 209–213.
5. Schiller, J., Schiller, Y. & Clapham, D. E. (1998) *Nat. Neurosci.* **1,** 114–118.
6. Zilberter, Y., Kaiser, K. M. & Sakmann, B. (1999) *Neuron* **24,** 979–988.
7. Isaacson, J. S. & Strowbridge, B. W. (1998) *Neuron* **20,** 749–761.
8. Bischofberger, J. & Jonas, P. (1997) *J. Physiol. (London)* **504,** 359–365.
9. Chen, W. R., Midtgaard, J. & Shepherd, G. M. (1997) *Science* **278,** 463–467.
10. Kirillova, V. & Lin, J. W. (1998) *Neuroscience* **87,** 255–264.
11. Bieda, M. C. & Copenhagen, D. R. (1999) *J. Neurophysiol.* **81,** 3092–3105.
12. Ivanov, A. I. & Calabrese, R. L. (2000) *J. Neurosci.* **20,** 4930–4943.
13. Pare, D., Shink, E., Gaudreau, H., Destexhe, A. & Lang, E. J. (1998) *J. Neurophysiol.* **79,** 1450–1460.
14. Svoboda, K., Denk, W., Kleinfeld, D. & Tank, D. W. (1997) *Nature (London)* **385,** 161–165.
15. Delaney, K. R. & Hall, B. J. (1996) *J. Neurosci. Methods* **68,** 193–202.
16. Ressler, K. J., Sullivan, S. L. & Buck, L. B. (1994) *Cell* **79,** 1245–1255.
17. MacLeod, K. & Laurent, G. (1996) *Science* **274,** 976–979.
18. Denk, W., Strickler, J. H. & Webb, W. W. (1990) *Science* **248,** 73–76.
19. Rall, W., Shepherd, G. M., Reese, T. S. & Brightman, M. W. (1966) *Exp. Neurol.* **14,** 44–56.
20. Denk, W., Delaney, K. R., Gelperin, A., Kleinfeld, D., Strowbridge, B. W., Tank, D. W. & Yuste, R. (1994) *J. Neurosci. Methods* **54,** 151–162.
21. Denk, W. & Svoboda, K. (1997) *Neuron* **18,** 351–357.
22. Svoboda, K., Helmchen, F., Denk, W. & Tank, D. W. (1999) *Nat. Neurosci.* **2,** 65–73.
23. Colbert, C. M., Magee, J. C., Hoffman, D. A. & Johnston, D. (1997) *J. Neurosci.* **17,** 6512–6521.
24. Hoffman, D. A., Magee, J. C., Colbert, C. M. & Johnston, D. (1997) *Nature (London)* **387,** 869–875.
25. Shen, G. Y., Chen, W. R., Midtgaard, J., Shepherd, G. M. & Hines, M. L. (1999) *J. Neurophysiol.* **82,** 3006–3020.
26. Desmaisons, D., Vincent, J. D. & Lledo, P. M. (1999) *J. Neurosci.* **19,** 10727–10737.
27. Takechi, H., Eilers, J. & Konnerth, A. (1998) *Nature (London)* **396,** 757–760.
28. Kovalchuk, Y., Eilers, J., Lisman, J. & Konnerth, A. (2000) *J. Neurosci.* **20,** 1791–1799.
29. Chen, W. R., Xiong, W. & Shepherd, G. M. (2000) *Neuron* **25,** 625–633.
30. Price, J. L. & Powell, T. P. (1970) *J. Cell Sci.* **7,** 631–651.
31. Helmchen, F., Svoboda, K., Denk, W. & Tank, D. W. (1999) *Nat. Neurosci.* **2,** 989–996.
32. Llinas, R. R. (1988) *Science* **242,** 1654–1664.
33. Johnston, D., Magee, J. C., Colbert, C. M. & Cristie, B. R. (1996) *Annu. Rev. Neurosci.* **19,** 165–186.
34. Chen, W. R. & Shepherd, G. M. (1997) *Brain Res.* **745,** 189–196.
35. Bhalla, U. S. & Bower, J. M. (1997) *J. Comput. Neurosci.* **4,** 221–256.
36. Bijlenga, P., Liu, J. H., Espinos, E., Haenggeli, C. A., Fischer-Lougheed, J., Bader, C. R. & Bernheim, L. (2000) *Proc. Natl. Acad. Sci. USA* **97,** 7627–7632.
37. Zucker, R. S. (1999) *Curr. Opin. Neurobiol.* **9,** 305–313.
38. Atluri, P. P. & Regehr, W. G. (1996) *J. Neurosci.* **16,** 5661–5671.
39. Delaney, K. R. & Tank, D. W. (1994) *J. Neurosci.* **14,** 5885–5902.
40. Swandulla, D., Hans, M., Zipser, K. & Augustine, G. J. (1991) *Neuron* **7,** 915–926.